Research Article – Vol. 02, Issue 04, No. 09

Bilijipublication

Advanced in Engineering and Intelligence Systems

Journal Web Page: https://aeis.bilijipub.com

Estimation of Ultimate Bearing Capacity in rock-socketed piles using optimized machine learning approaches

Ali Hassan[1, *], Hamza Rashid[1]

[1] *Department of Mechatronics Engineering, center of Industrial Electronics (CIE), University of Southern Denmark, Sønderborg, Denmark*

Highlights

- Introduction of an innovative methodology using the Naive Bayes algorithm for precise prediction of Ultimate Bearing Capacity (Q_u) in rock-socketed piles.
- Integration of state-of-the-art meta-heuristic algorithms (Artificial Hummingbird Algorithm and Improved Grey Wolf Optimizer) to enhance model precision.
- Development of three distinct models (NBAH, NBIG, and NB hybrid models) for predicting Q_u in rock-socketed piles.
- Assessment of model performance using various evaluators, including R2, RMSE, RSR, MAE, WAPE, and SI.
- Highlighting the standout performance of the NBIG model with a remarkable R2 value of 0.993 and an ideal RMSE of 1381.3 during the training phase, emphasizing its accuracy in predicting Q_u.

Article Info

Received: 30 November 2023
Received in revised: 25 December 2023
Accepted: 30 December 2023
Available online: 31 December 2023

Keywords

Ultimate Bearing Capacity;
Naive Bayes;
Artificial;
Hummingbird Algorithm;
Improved Grey Wolf optimizer

Abstract

Rock-socketed piles, frequently employed in soft ground foundations, represent a matter of paramount issue in research, design, and construction, primarily because of their bearing capacity. The precise estimation of the Ultimate Bearing Capacity (Q_u) of these rock-socketed piles proves to be a formidable challenge, primarily due to the inherent uncertainties associated with the myriad factors influencing this capacity. This article introduces an innovative methodology for the precise prediction of Q_u. This approach leverages the Naive Bayes (NB) algorithm to construct exact and comprehensive predictive models. To enhance the model's precision, the study incorporates two state-of-the-art meta-heuristic algorithms, the Artificial Hummingbird Algorithm (AHA) and the Improved Grey Wolf Optimizer ($IGWO$), into the analysis. This amalgamation gives rise to three distinct models: $NBAH$, $NBIG$, and the NB hybrid models. Moreover, the implemented method is assessed against the results obtained from experiments by some evaluators including R^2, RMSE, RSR, MAE, WAPE, and SI. Of these models, the $NBIG$ model emerges as a standout performer, boasting remarkable R^2 value of 0.993 (lower than 1% enhanced performance compared to NBAH) and an ideal $RMSE$ of 1381.3 (about 16% lower than that of NBAH) during the training phase. These impressive metrics underscore the model's exceptional accuracy and unwavering dependability in predicting the Q_u of rock-socketed piles.

Nomenclature

Indices		*RMSE*	*Root Mean Square Error*
Q_u	*Ultimate Bearing Capacity*	*MAE*	*Mean Absolute Error*
NB	*Naive Bayes*	*RSR*	*Ratio of RMSE*
AI	*Artificial intelligence*	*WAPE*	*Weight Absolute Percentage Error*
AHA	*Artificial Hummingbird Algorithm*	*SI*	*Scatter Index*
IGWO	*Improved Grey Wolf Optimizer*	***Parameters***	
ML	*Machine Learning*	R^2	*coefficient of determination*

1. Introduction

* Corresponding Author: Ali Hassan
Email: alhas23@student.sdu.dk

Pile foundations are the unsung heroes of construction, silently bearing the weight and loads of structures deep within the earth. Ensuring the stability and safety of these structures heavily relies on accurately estimating the ultimate bearing capacity (Q_u) of these piles. Over the years, a plethora of experimental and theoretical methods have been developed to predict this vital parameter [1]– [5]. However, the intricate nature of piles, coupled with the limitations of existing models, often leaves engineers seeking more precise solutions. Moreover, many existing methods are tailored to specific construction sites, rendering them less versatile. Among the available techniques, the Static Load Test (SLT) stands out as the gold standard for determining Q_u[6]– [8]. While it offers reliable results, the SLT is labor-intensive, expensive, and time-consuming. In recent years, High Strain Dynamic Testing ($HSDT$) has emerged as a cutting-edge alternative for predicting Q_u. This innovative method leverages wave propagation theory and utilizes a pile-driving analyzer (PDA) to assess a pile's capacity. Previous research has demonstrated a strong correlation between the bearing capacity estimates obtained through PDA and those derived from SLT, suggesting the method's reliability[9]–[11]. One of the significant advantages of $HSDT$ is its efficiency and cost-effectiveness compared to the traditional SLT. Additionally, it provides real-time insights into pile behavior during installation, making it an attractive option for engineers[12]. However, a challenge remains: $HSDT$ often requires multiple tests per project, which can increase costs and project duration. Recognizing this limitation, engineers and researchers are turning to Artificial Intelligence (AI) as a potential solution. AI technologies promise more accurate and efficient predictions by analyzing vast datasets and expediting complex engineering tasks. By combining the efficiency of $HSDT$ with the precision and speed of AI, engineers hope to optimize construction projects by reducing the number of tests required and streamlining engineering processes[13]–[16].

Machine learning (ML) models, a subset of AI, have gained prominence in geotechnical engineering for their ability to handle large datasets and uncover intricate patterns[17]– [19]. Predicting the Q_u of piles with ML involves the following key steps:

- Data Collection: Gather comprehensive data related to piles, including information on soil properties, pile geometry, load test results, and any other relevant variables. This dataset is the foundation for training and validating the ML model[20].
- Feature Engineering: Carefully select and preprocess the features (input variables) most likely to influence pile capacity. This step may involve data cleaning, normalization, and feature selection techniques to improve the model's performance.
- Model Selection: Choose an appropriate ML algorithm or combination of algorithms for the estimation task. Frequently selected alternatives encompass regression models, Naive Bayes (NB), support vector machines, and neural networks.
- Training and Validation: Split the dataset into training and validation sets to train the model and assess its performance. Iteratively fine-tune the model's hyperparameters to optimize its predictive accuracy.
- Testing: Upon successful training and validation of the model, it can be tested on new, unseen data to evaluate its predictive capabilities. This step helps ensure the model's generalizability to different construction scenarios.
- Deployment: Implement the trained ML model into practical engineering workflows. Engineers can use it to make predictions about Q_u quickly and accurately, reducing the reliance on costly and time-consuming physical tests[21].

By integrating ML into the prediction of Q_u, engineers can harness the power of data-driven insights to make more informed decisions in pile foundation design[22]–[25]. For instance, researchers used NB machine learning method in the case of underground soil-structure interaction [26] and mechanical properties of steel strand.[27] This approach reduces costs and project timelines and enhances construction projects' overall safety and efficiency. As AI technologies continue to advance, they are poised to revolutionize the field of geotechnical engineering, providing engineers with valuable tools for the complex challenges they face in the world of construction[28].

In pursuit of accurate and highly reliable predictive outcomes, this study introduces a groundbreaking approach that converges the realms of ML and AI. The unique hybridization technique employed in this study has been meticulously crafted to enhance the efficacy of NB models, ensuring the generation of results that can be unequivocally trusted. These pioneering hybrid models have eclipsed conventional methodologies by amalgamating two state-of-the-art and potent optimization techniques, signifying a substantial leap forward in this domain. The models underwent a comprehensive comparative analysis, evaluating their performance in isolation and hybrid configurations. Furthermore, the

deliberate decision to integrate two distinct optimizers, namely the Artificial Hummingbird Algorithm (AHA) and the Improved Grey Wolf Optimizer ($IGWO$), into the development of these hybrid models was undertaken to harness the unique strengths of each optimizer. This strategic amalgamation culminated in a level of performance that far surpassed expectations, underlining the superiority of this hybrid approach. Moving beyond the technical aspects, this study also contemplated the pragmatic implications of these findings within real-world applications. The heightened precision attained through these hybrid models can significantly enhance the decision-making processes in geotechnical engineering projects. This serves to mitigate the risks associated with inaccurate estimations of Q_u, offering a tangible benefit to the field of geotechnical engineering. NB is chosen in order to capitalize on its simplicity, speed, and efficiency, particularly when faced with limited data. Its ease of implementation and computational efficiency make it ideal for quick predictions, while its probabilistic nature accommodates uncertainty in classification tasks, provided the assumption of feature independence holds.

2. Materials and Methodology

2.1. Data gathering

The ongoing research is centered around establishing a comprehensive database to facilitate the development of predictive models for the Ultimate Bearing Capacity (Q_u) of rock-socketed piles. This endeavor involves the execution of Standard Penetration Test (SPT) assessments on these piles. To enhance the efficiency of this analysis, the study thoughtfully divides the dataset into three distinct subsets: training (70%), validation (15%), and testing (15%). This research builds upon a dataset comprising 172 experimental samples from prior studies. This dataset validates the empirical distribution method and fortifies the predictive models being utilized. By employing the Naive Bayes (NB) model, this study investigates the behavior of Q_u by harnessing the inherent predictive capabilities of the variables outlined in Table 1. The meticulous selection of input parameters, which are predictor variables, is paramount. Previous research has highlighted that the most influential factor affecting Q_u is the geometric attributes of the piles, particularly their length and diameter. To account for the interaction between soil and rock layers, two specific geometric ratios were chosen: the ratio of length in the soil layer (L_s) to socket length (L_r), and the ratio of the total length (L_p) to diameter (D) and reference depth in rock layers (H_r), a reference point for various geotechnical calculations[29]. Apart from the pile's physical dimensions, previous studies have identified other parameters that significantly impact predictive models for pile-bearing capacity, such as rock strength (UCS) and the Standard Penetration Test N-value (SPT N-value). In this study, the SPT N-value was meticulously selected as an input parameter to account for the influence of the soil layer on Q_u. To summarize, the model inputs used for predicting Q_u in rock-socketed piles consist of L_s/L_r, L_p/D, UCS, and $N-SPT$. As depicted in Fig. 1, the histogram plot effectively visualizes the relationships between input and output parameters. Lower values of H_r, $N-SPT$, and L_p/D are correlated with higher Q_u values, while higher UCS and L_s/L_r values tend to increase Q_u. In essence, all input parameters exert an influence on Q_u values [30], [31].

Table 1. The statistical properties of the input variable of Q_u.

Variables	Indicators				
	Category	Min	Max	Avg	St. Dev.
Lp/D	Input	4.331	0.286	0	0
Ls/Lr	Input	96.3	31.7	166.4	68.5
N_SPT	Input	31.34	4.9	44.7	24.2
UCS	Input	22.44	5.7	59.6	23.5
Hr	Input	4.331	0.286	0	0
Qu	Output	96.3	31.7	166.4	68.5

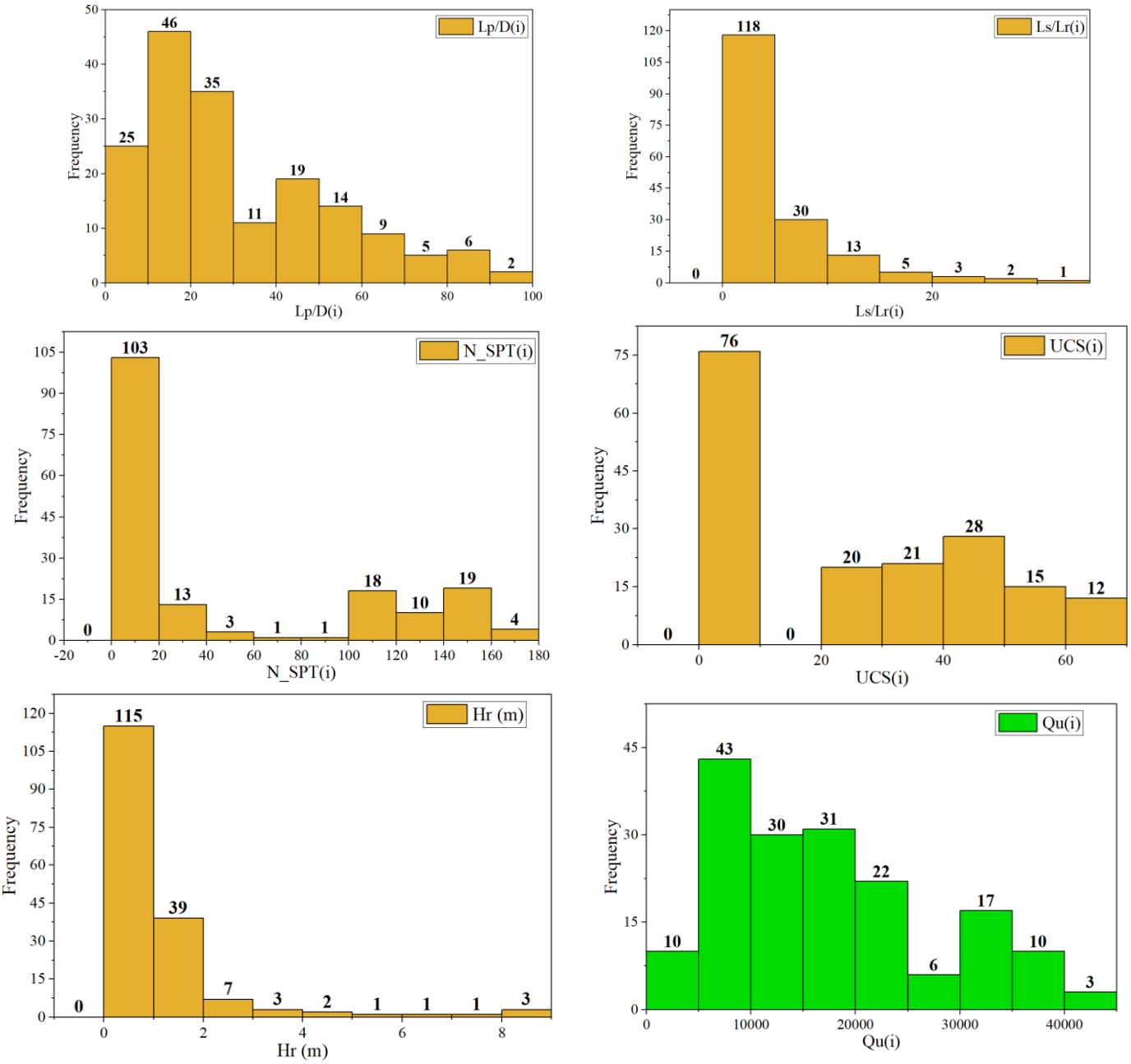

Fig. 1. The histogram plot between input and output

2.2. Naive Bayes (NB)

The Naive Bayes (NB) classifier, a probabilistic type, employs Bayes' theorem and assumes robust feature independence[32]. Its key strength lies in its straightforward design, obviating the need for intricate iterative parameter estimation techniques. Additionally, it is noted by Das et al. that the NB classifier is resilient to noise and irrelevant attributes[33]. The NB classifier is based on the following equation:

$$y = \underset{y_i=\{landslide,non-landslide\}}{\arg\max} P(y_i) \prod_{i=1}^{14} P\left(\frac{x_i}{y_i}\right) \quad (1)$$

where $P(y_i)$is the prior probability of y_i, $P(\frac{x_i}{y_i})$is the posterior probability, and it can be calculated by:

$$P\left(\frac{x_i}{y_i}\right) = \frac{1}{\sqrt{2\pi\sigma}} e^{\frac{-(x_i-\mu)^2}{2\sigma^2}} \quad (2)$$

Where μ is the mean and σ is the standard deviation of x_i.

2.3. Artificial Hummingbird Algorithm (AHA)

The Artificial Hummingbird Optimization Approach (AHA) draws inspiration from hummingbirds' flight and foraging behaviors to optimize complex functions efficiently. AHA details. Hummingbirds employ three flight skills (axial, diagonal, omnidirectional) and various foraging strategies (guided, territorial, migratory) for efficient navigation. A visitation table in AHA mimics their memory to prevent revisiting locations, focusing on unexplored areas.

A computational method called the *AHA* is inspired by the foraging and flight patterns of hummingbirds. Three main models of this algorithm are presented in this study [34], [35].

2.3.1. Guided foraging

The current foraging model has used three different flight behaviors: axial, diagonal, and omnidirectional flight[36], [37]. The following method can derive a mathematical expression representing guided foraging and a potential food source.

$$v_i(t+1) = x_{i,ta}(t) + h.b.\left(x_i(t) - x_{i,ta}(t)\right) h{\sim}N(0,1) \quad (3)$$

The Eq. (3) defines $x_{i,ta}(t)$ as the spatial coordinates of the desired food source, with h signifying the guiding parameter[38]. Additionally, $x_i(t)$ represents the location of the ith food source in the temporal domain, which is illustrated in Eq. (4).

$$x_{Ai}(t) = \begin{cases} x_i(t) & f(x_i(t)) \le f(v_i(t+1)) \\ v_i(t+1) & f(x_i(t)) > f(v_i(t+1)) \end{cases} \quad (4)$$

2.3.2. Territorial foraging

Studies show that hummingbirds prefer finding new food sources instead of switching between available ones once their current source is depleted. This behaviour is emulated in the guided foraging aspect of the AHA algorithm. Furthermore, hummingbirds display territorial foraging behaviour by exploring nearby areas within their territory to discover potentially improved solutions. This behaviour is integrated into the guided foraging module of the AHA algorithm, as defined in Eq. (5):

$$v_i(t+1) = x_i(t) + g.b.\left(x_i(t)\right) g \sim N(0,1) \quad (5)$$

2.3.3. Migration foraging

Eq. (6) is where the idea of migration foraging was developed.

$$x_{war}(t+1) = lb + r.(ub - lb) \quad (6)$$

The variable x_{war} is used to denote the source of sustenance possessing the poorest population rate of nectar refilling. Meanwhile, *lower* limit lb and *upper* limit ub ranges are established, assuming that a factor denoted by the letter r is random[39].

2.4. Improved Grey Wolf Optimizer (IGWO)

IGWO, a novel population-based synthetic optimization algorithm, leverages the hunting strategies of a wolf pack to pursue and explore optimization objectives. It is crucial to note that there exists a rigid social structure among wolves, where pack members are categorized into four distinct groups based on their social status, namely Alpha (α), beta (β), delta (δ), and omega (ω). As depicted in Figure 2, the Alpha assumes the role of the leader and supreme authority within the pack, responsible for determining hunting and resting times and locations. The Beta occupies the second tier of the hierarchy, assisting the Alpha in decision-making and managing the pack's behavior. The Delta initially shoulders responsibilities related to security, upkeep, and marking[40]. Within this hierarchy, the Delta follows the directives of the Alpha and Beta. Finally, at the lowest rank of the hierarchy, the Omega represents wolves that do not fall into the aforementioned three classes. This hierarchical structure within the wolf pack significantly influences the hunting process, with the Delta and Beta collaborating in hunting and prey encirclement under the Alpha's guidance.

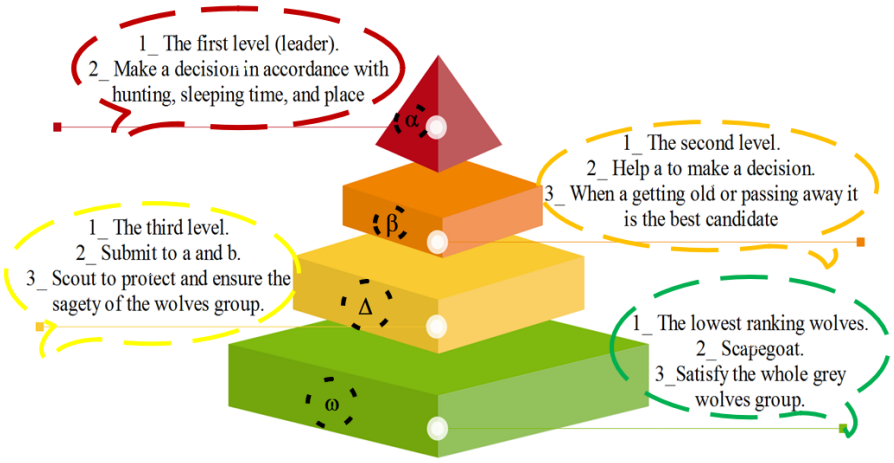

Fig. 2. Hierarchy of the IGWO algorithms

An individual's coolness is eventually replaced by a pack of wolves changing their movements to catch prey as it flees. During the hunting process, gray wolves employ a strategy where they encircle their prey in the following manner:

$$\vec{C} = \left|\vec{O} \times \vec{L}_{prey}(r) - \vec{L}_{wolf}(r)\right| \quad (7)$$

Here, r is the current's repetition, $\vec{L}_{prey}, \vec{L}_{wolf}$ identify the position of prey, O represents the factor responsible for oscillations and its formula for computation are described as follows:

$$\vec{O} = 2\vec{t}_1 \quad (8)$$

Updating the formula for the gray wolf's position would look like this:

$$\vec{L}_{wolf}(r+1) = \vec{L}_{prey}(r) - \vec{I} \times \vec{D} \quad (9)$$

Where, $\vec{I}$ shows the isotropic coefficient specified based on Eq. (10):

$$\vec{I} = 2a \times \vec{t}_2 - a \quad (10)$$

t_1 and t_2 are random vectors in the range of [0,1], a decreases linearly from 2 to 0 with increasing iteration time[41].

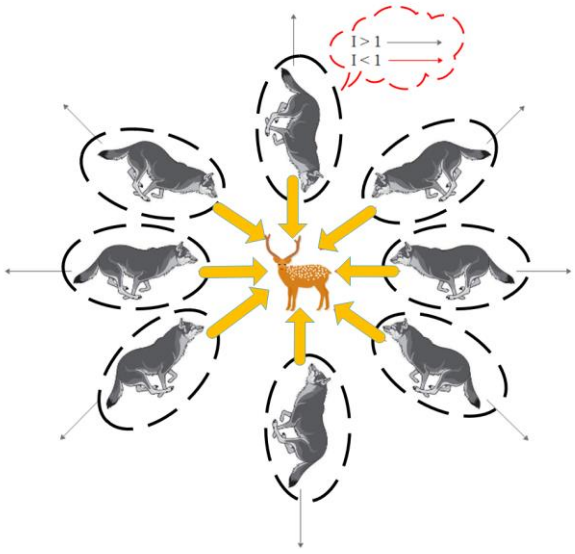

Fig. 3. Vectors' possible next position and their position

Grey wolves engage in hunting and update their positions using the provided formula. However, adjustments in values E and F enable wolves to adopt more optimal individual positions. As depicted in Figure 3, wolves initiate approaches and attacks on prey when the value of I is less than 1. When necessary, a wolf may be compelled to abandon its current prey and search for an alternative. It's worth noting that the precise location of prey within the analyzed space remains unknown, making alpha, beta, and delta the optimal solutions, as exemplified in Figure 4. Additionally, other gray wolves should adjust their positions according to the following formula:

$$\begin{cases} \vec{B}_{Alpha} = \left|\vec{O}_1 \times \vec{Y}_{Alpha}(r) - \vec{Y}\right| \\ \vec{B}_{Beta} = \left|\vec{O}_2 \times \vec{Y}_{Beta}(r) - \vec{Y}\right| \\ \vec{B}_{Delta} = \left|\vec{O}_3 \times \vec{Y}_{Delta}(r) - \vec{Y}\right| \end{cases} \tag{11}$$

$$\begin{cases} \vec{Y}_1 = \vec{Y}_{Alpha} - \vec{Y}_1 \times \vec{D}_{Alpha} \\ \vec{Y}_2 = \vec{Y}_{Beta} - \vec{Y}_2 \times \vec{D}_{Beta} \\ \vec{Y}_3 = \vec{Y}_{Delta} - \vec{Y}_3 \times \vec{D}_{Delta} \end{cases} \tag{12}$$

$$\vec{Y}(r+1) = \frac{\vec{Y}_1 + \vec{Y}_2 + \vec{Y}_3}{3} \tag{13}$$

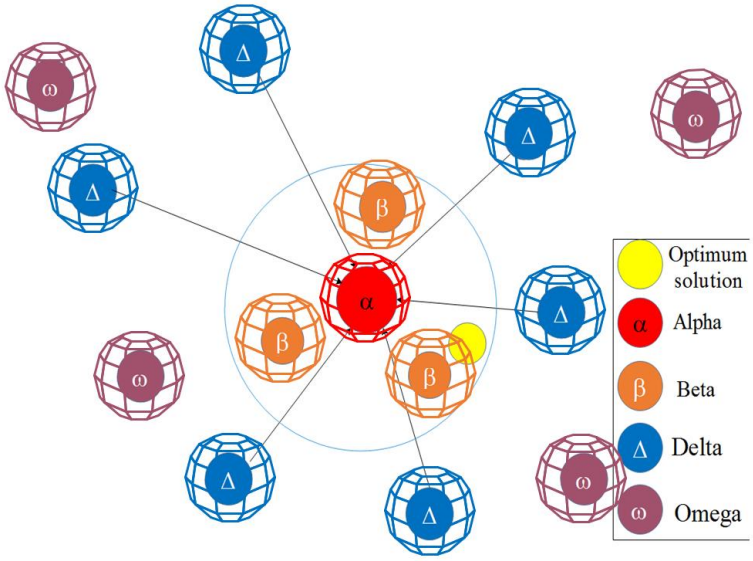

Fig. 4. Hierarchical mechanism of the IGWO

2.5. Performance evaluation methods

This article employs a range of metrics to assess the models, including Root Mean Square Error ($RMSE$), Correlation Coefficient (R2), Mean Absolute Error (MAE), Weight Absolute Percentage Error ($WAPE$), Ratio of RMSE (RSR), and scattered index (SI), as previously outlined. A high R2 value signifies exceptional algorithm performance throughout the training, validation, and testing phases. Conversely, lower $RMSE$ and MAE values are preferable, as they indicate decreased model errors. These metrics are computed using Eqs. (14) to (19).

Correlation Coefficient

$$R^2 = \left(\frac{\sum_{i=1}^{W}(h_i - \bar{h})(q_i - \bar{q})}{\sqrt{[\sum_{i=1}^{W}(h_i - h)^2][\sum_{i=1}^{W}(q_i - \bar{q})^2]}} \right)^2 \tag{14}$$

Root Mean Square Error

$$RMSE = \sqrt{\frac{1}{W}\sum_{i=1}^{W}(q_i - h_i)^2} \tag{15}$$

Mean Absolute Error

$$MAE = \frac{1}{W}\sum_{i=1}^{W}|q_i - h_i| \tag{16}$$

Ratio of RMSE

$$RSR = \frac{RMSE}{St.Dev.} \tag{17}$$

Weight Absolute Percentage Error

$$WAPE = \max\left[\frac{|q_i - h_i|}{q_i}\right] \tag{18}$$

Scatter index

$$SI = \frac{RMSE}{\bar{q}} \quad (19)$$

In these equations, h_i and q_i refer to the predicted and experimental values, respectively. The mean values of the experimental samples and predicted are represented by $\bar{h}$ and $\bar{q}$. Alternatively, W denotes the number of samples being considered.

3. Results and discussion

In this study, three models (NB, $NBIG$, and $NBAH$) were employed to forecast Q_u. The performance evaluation was carried out across four distinct phases: training (70%), validation (15%), testing (15%), and All (100%). This careful distribution of data was employed to ensure a fair evaluation of the models, ultimately resulting in more accurate and reliable Q_u estimates for improved soil analysis and decision-making in engineering and construction projects. Table 2 shows statistical metrics for evaluation: $WAPE, MAE,$ R2, $RMSE$, and RSR.

- R^2: R^2 values indicate the degree to which the independent variable accounts for the variance in the dependent variable. During the training phase, the $NBIG$ model exhibited exceptional predictive accuracy with an outstanding R^2 value of 0.993, surpassing its counterparts. In contrast, the NB model showed slightly lower R^2 values during training, with a measurement of 0.976.
- RMSE: $RMSE$ values ranged from 1381.3 to 3467.3. Notably, during testing, the NB model displayed the highest $RMSE$, while the $NBIG$ model showcased the lowest $RMSE$ during training.
- RSR: The RSR metric indicated the highest value of 0.341 for the NB model during the training phase, whereas the $NBIG$ model achieved the minimum value of 0.137 during the training stage.
- MAE: For MAE, the NB model exhibited the highest value at 2147.57, while the $NBIG$ model emerged as the frontrunner, presenting the most favorable MAE values of 1048.63 during the training phase.
- WAPE: The $NBIG$ model demonstrated the lowest and most favorable $WAPE$ value of 0.061 during the training phase, while the NB model had the highest $WAPE$ value of 0.137 during the validation phase.
- SI: The NBIG model registered the best applicability in predicting with possessing the lowest SI value of 0.798 in the training phase. On the other hand, The NB model identified as the weakest model.

Overall, the comprehensive findings unequivocally establish the $NBIG$ model's superiority over NB and $NBAH$ across multiple evaluation phases. This approach ensures robust soil analysis and contributes to more informed decision-making in engineering and construction projects.

Table 2. The result of developed models for NB.

Model	Phase	Index values					
		RMSE	R^2	MAE	RSR	WAPE	SI
NB	Train	3709.1	0.976	2544.25	0.367	0.147	0.2142
	Validation	3996.6	0.970	2783.32	0.402	0.137	0.1971
	Test	3467.3	0.963	2147.57	0.341	0.143	0.2302
	All	3718.9	0.973	2520.43	0.365	0.145	0.2135
NBIG	Train	1381.3	0.993	1048.63	0.137	0.061	0.0798
	Validation	2137.4	0.983	1743.60	0.215	0.086	0.1054
	Test	1874.1	0.991	1492.95	0.184	0.099	0.1244
	All	1597.7	0.990	1220.85	0.157	0.070	0.0917
NBAH	Train	1657.1	0.986	1118.26	0.164	0.065	0.095
	Validation	2286.7	0.973	1684.02	0.230	0.083	0.1128
	Test	1940.3	0.976	1363.25	0.191	0.091	0.1288
	All	1809.8	0.982	1240.81	0.177	0.071	0.1039

Fig. 5 displays a scatter plot that provides a visual representation of our analysis. This plot showcases hybrid models assessed through the metrics of R2 and $RMSE$. Notably, the $NBIG$ model stands out for its exceptional accuracy, evident in the tight clustering of data points around the central line with minimal spread. Furthermore, it is worth highlighting that the $RMSE$ value for the validation data proves to be lower than that for the testing data, which indicates a reduction in data dispersion and bolsters the model's precision. On the other hand, the NB

model, while certainly valuable, exhibits a somewhat lower level of accuracy, resulting in a more scattered distribution of output when compared to the other models.

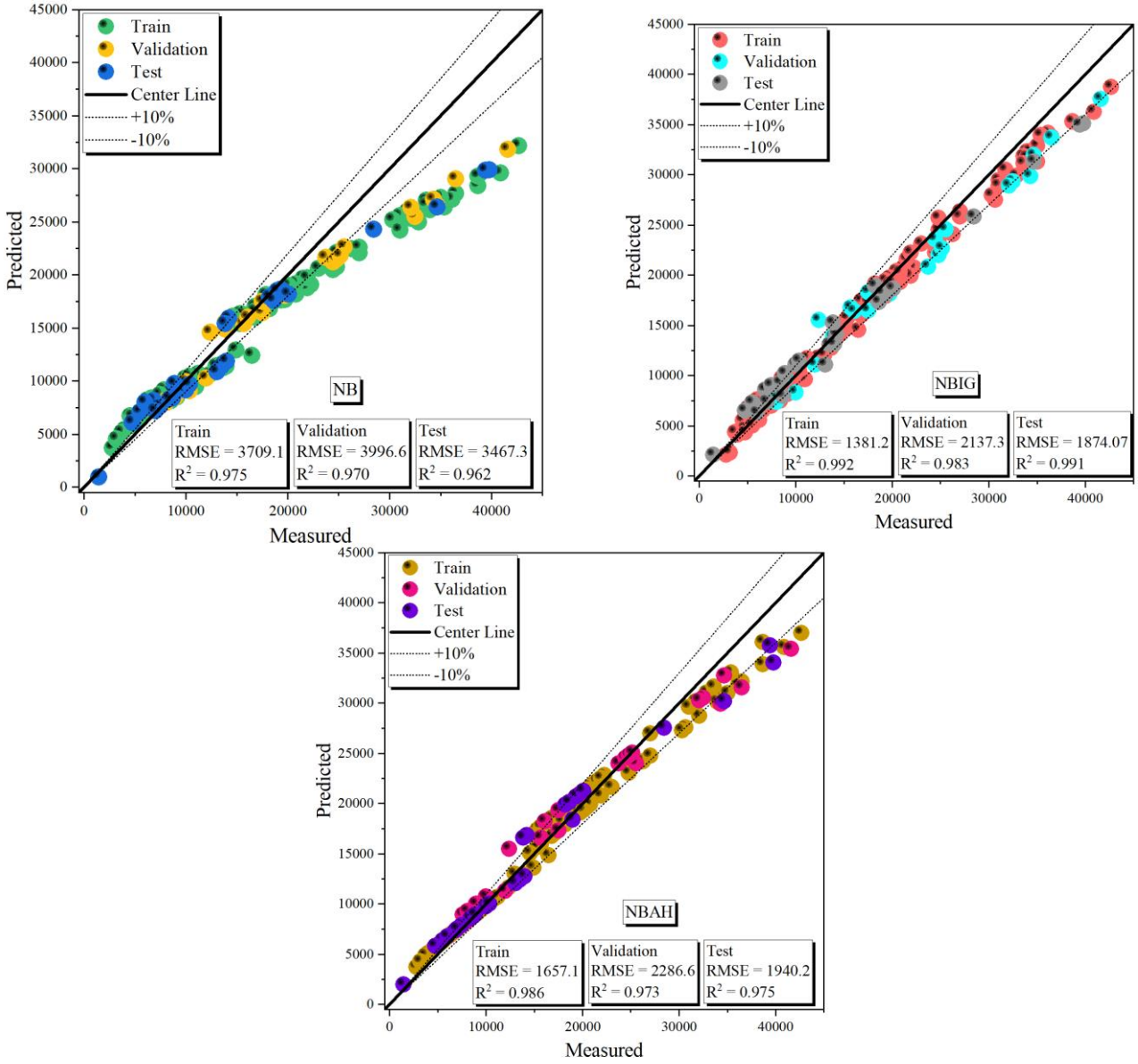

Fig. 5. The scatter plot for developed hybrid models.

In Fig. 6, the study presents a comparative visualization of the predicted and observed Q_u through a line plot. This graphical representation is segmented into three main phases: training, validation, and testing. The accuracy of this portrayal depends on how closely the predicted behavior aligns with the observed behavior. Within these three phases, subtle discrepancies are apparent, primarily stemming from the prominent positioning of predicted points above the measured values within the *NBIG* model. In contrast, the *NB* and *NBAH* models reveal slight divergences between the projected and observed points, although their precision falls short of the level demonstrated by the *KNGT* model.

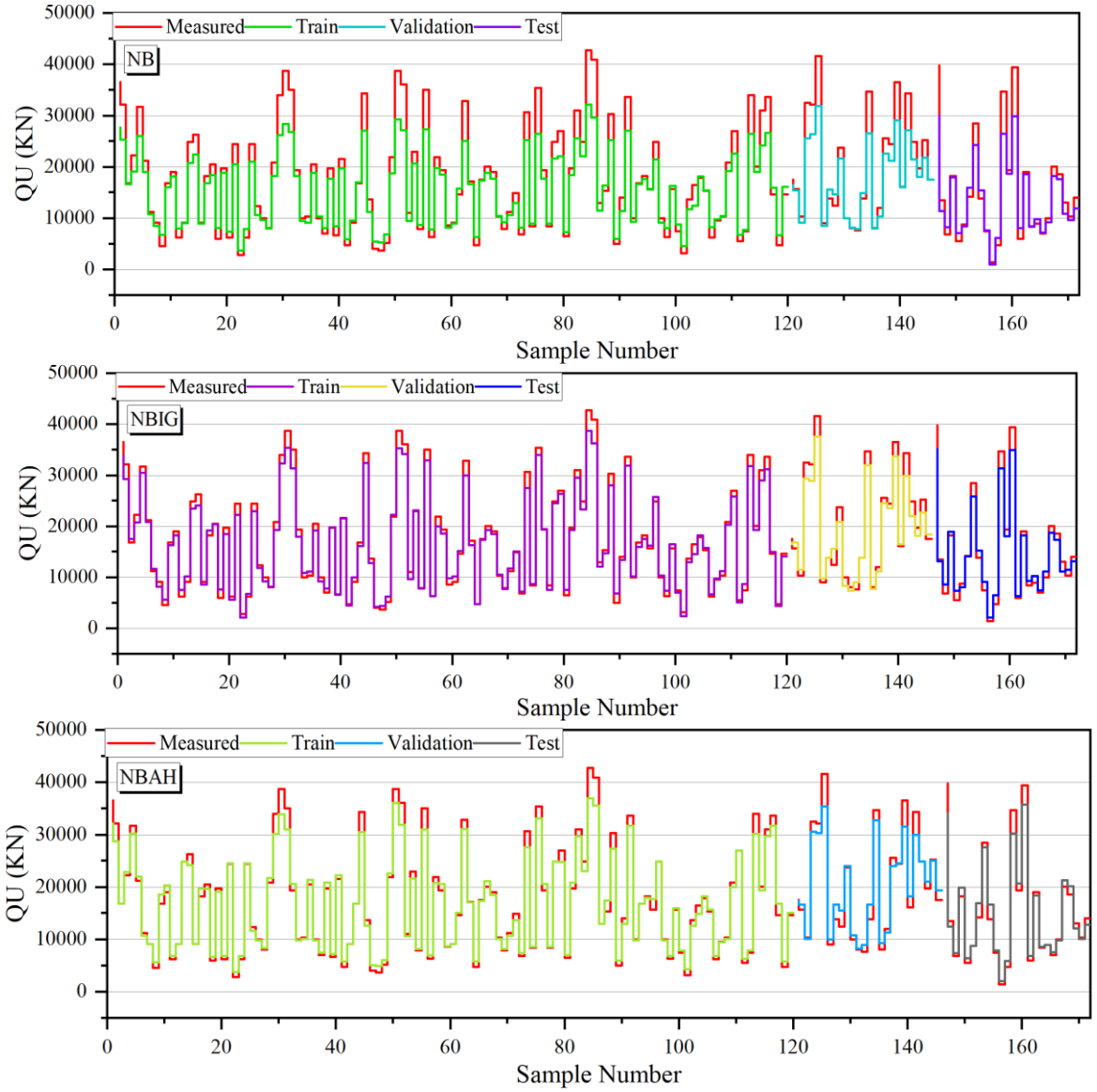

Fig. 6. The comparison of measured and predicted values.

Fig. 7 provides a visual representation of the error rate percentages for the hybrid models, employing a histogram plot. It is noteworthy that the samples tend to congregate within a relatively narrow error range of −10% to 10%, demonstrating the consistent and closely grouped frequencies observed in the $NBIG$ model. Among the three models in consideration, the NB model distinguishes itself by displaying a broader range of error percentages from −30% to 30%. This broader range signifies increased variability and a decreased level of predictive precision compared to the other two models.

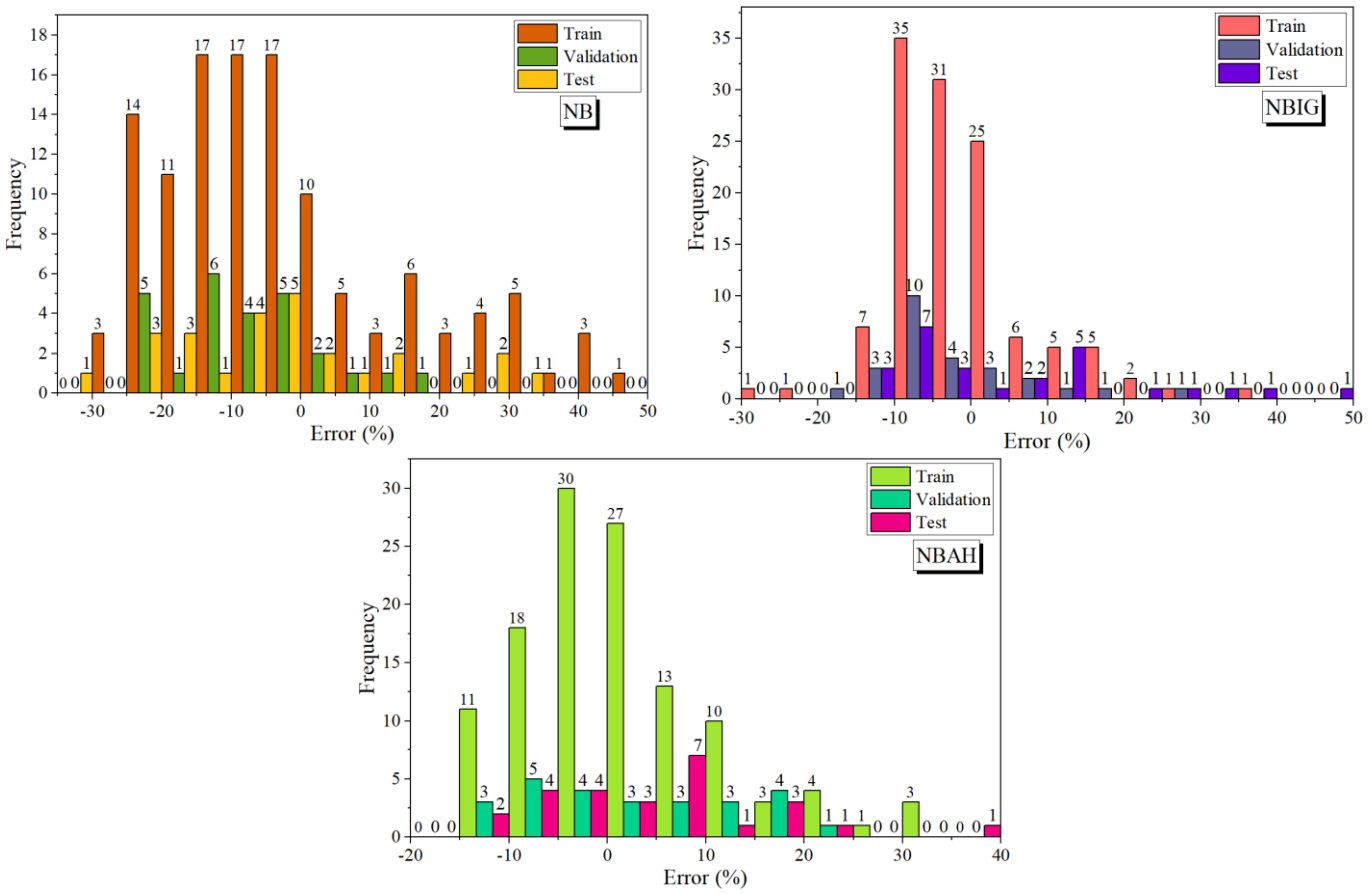

Fig. 7. The error rate percentage for the hybrid models is based on a histogram plot.

Moreover, in Fig. 8, a scatter plot showcases the developed models' error percentages. As mentioned earlier, these models have undergone assessment across three distinct phases. The visual representation unequivocally indicates that these models consistently exhibited commendable performance, maintaining error rates below ten percent. It is worth highlighting that the NBIG model achieved exceptional accuracy, demonstrating errors approaching zero percent. In contrast, the NB model displayed slightly more variability, with its highest error reaching 50%.

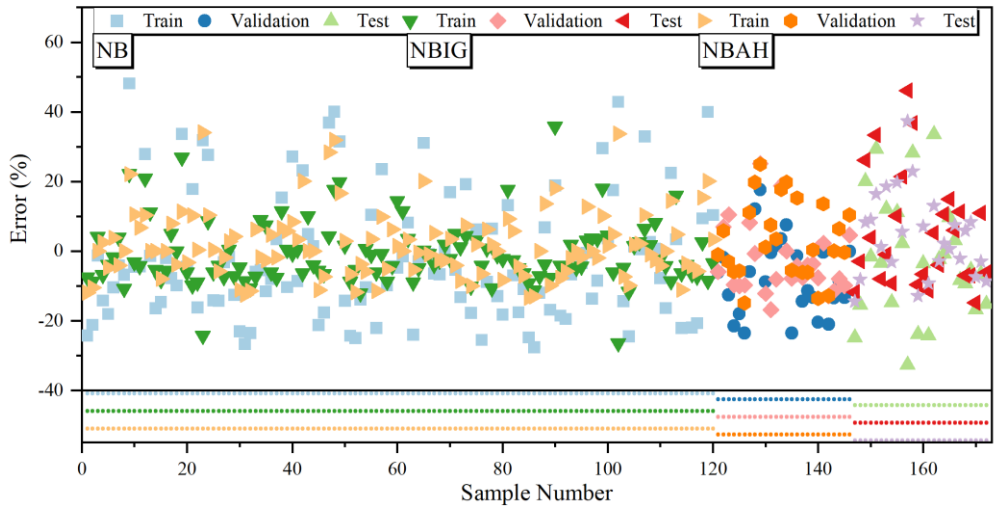

Fig. 8. The scatter plot of errors among the developed models.

The exhibition of Taylor diagrams for the applied NB, NBIG, and NBAH predictive models is shown in Fig. 9. This diagram is a statistical summary of the observed and predicted Q_u, which combines the root mean square errors (RMSE), correlation coefficients (CC), and the normalized standard deviations. From the figure demonstration, the NBIG model (Combination of the NB model and IGWO optimizer) is considered as the best predictive model, and its results are closest to the ideal benchmark observed experimental data.

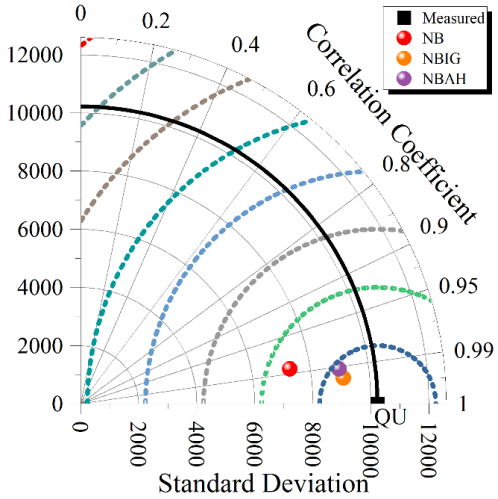

Fig. 9. The Taylor diagram for related models.

4. Conclusion

This study presents a groundbreaking approach for the precise prediction of Ultimate Bearing Capacity (Q_u) values, harnessing the capabilities of Machine Learning (ML) techniques, with a specific focus on Naive Bayes (NB) algorithms. This innovative methodology not only offers a cost-effective alternative but also significantly reduces the time required for Q_u predictions. At its core, this Q_u prediction framework revolves around a novel ML model based on the NB algorithm, showcasing its potential to reshape Q_u prediction practices. To further enhance accuracy and minimize errors, two meta-heuristic algorithms, $IGWO$ and AHA, were thoughtfully integrated into the process, leading to the creation of three distinct models: $NBIG, NBAH$, and an individual NB model. The validation of these models involved using laboratory samples obtained from reputable sources, spanning the training, validation, and testing phases. A comprehensive set of evaluation metrics, including R^2, $RMSE, MAE, RSR$, and $WAPE$, was employed to assess and compare model performance.

The results of this study notably indicate that the $NBIG$ models consistently achieved the highest R^2 value of 0.993, underscoring their superior predictive capabilities. Conversely, the standalone NB model exhibited the lowest R2 value, with a marginal difference of merely 2%.

Across all phases, $NBIG$ demonstrated exceptional performance by consistently yielding significantly lower $RMSE$ values (minimum value of 1382.3), with an outstanding 92% reduction compared to NB during Q_u prediction.

In terms of MAE, the $NBIG$ models emerged as clear frontrunners, delivering a remarkable 75% reduction in error compared to the NB model during the precise forecasting of Q_u .

While RSR and $WAPE$ metrics were used to assess model performance comprehensively, the $NBIG$ model consistently outperformed its counterparts during all phases.

The effectiveness of ML models as a trustworthy substitute for conventional experimental techniques for predicting Q_u, offering significant time and resource savings, is highlighted by this study's conclusion. Notably, the addition of the $IGWO$ optimizer makes these models even more effective, creating a cooperative relationship that consistently produces precise Q_u predictions. This innovative approach has the potential to revolutionize Q_u prediction methods in a variety of engineering and construction applications, ultimately enabling more informed resource allocation and decision-making procedures.

REFERENCES

[1] A. Kordjazi, F. P. Nejad, and M. B. Jaksa, “Prediction of ultimate axial load-carrying capacity of piles using a support vector machine based on

CPT data," *Comput Geotech*, vol. 55, pp. 91–102, 2014.
[2] M. F. Randolph, "Science and empiricism in pile foundation design," *Géotechnique*, vol. 53, no. 10, pp. 847–875, 2003.
[3] G. Likins and F. Rausche, "Correlation of CAPWAP with static load tests," in *Proceedings of the seventh international conference on the application of stresswave theory to piles*, 2004, pp. 153–165.
[4] E. Momeni, R. Nazir, D. J. Armaghani, and H. Maizir, "Prediction of pile bearing capacity using a hybrid genetic algorithm-based ANN," *Measurement*, vol. 57, pp. 122–131, 2014.
[5] M. A. Shahin, M. B. Jaksa, and H. R. Maier, "Artificial neural network applications in geotechnical engineering," *Australian geomechanics*, vol. 36, no. 1, pp. 49–62, 2001.
[6] M. Mansouri, M. Imani, and A. Fahimifar, "Ultimate bearing capacity of rock masses under square and rectangular footings," *Comput Geotech*, vol. 111, pp. 1–9, 2019.
[7] Y. Zhang, K. H. Andersen, and G. Tedesco, "Ultimate bearing capacity of laterally loaded piles in clay–Some practical considerations," *Marine Structures*, vol. 50, pp. 260–275, 2016.
[8] D. Chakraborty and J. Kumar, "Bearing capacity of foundations on slopes," *Geomechanics and Geoengineering*, vol. 8, no. 4, pp. 274–285, 2013.
[9] S. S. Tezcan, A. Keceli, and Z. Ozdemir, "Allowable bearing capacity of shallow foundations based on shear wave velocity," *Geotechnical & Geological Engineering*, vol. 24, pp. 203–218, 2006.
[10] J. Liu *et al.*, "Investigation of ultimate bearing capacity of shield tunnel based on concrete damage model," *Tunnelling and Underground Space Technology*, vol. 125, p. 104510, 2022.
[11] R. Zhang and X. Xue, "Determining ultimate bearing capacity of shallow foundations by using multi expression programming (MEP)," *Eng Appl Artif Intell*, vol. 115, p. 105255, 2022.
[12] K. Kuwajima, M. Hyodo, and A. F. Hyde, "Pile bearing capacity factors and soil crushabiity," *Journal of geotechnical and geoenvironmental engineering*, vol. 135, no. 7, pp. 901–913, 2009.
[13] A. Akbari Garakani, B. Heidari, S. Mokhtari Jozani, and O. Ghasemi-Fare, "Numerical and analytical study on axial ultimate bearing capacity of fixed-head energy piles in different soils," *International Journal of Geomechanics*, vol. 22, no. 1, p. 04021258, 2022.
[14] K. Khan *et al.*, "PCA-based hybrid intelligence models for estimating the ultimate bearing capacity of axially loaded concrete-filled steel tubes," *Materials*, vol. 15, no. 18, p. 6477, 2022.
[15] L. Zhu and H. Ma, "Study on the rupture surface morphology and ultimate bearing capacity of a self-anchored test pile," *Sci Rep*, vol. 12, no. 1, p. 16382, 2022.
[16] F. Masoumi, S. Najjar-Ghabel, A. Safarzadeh, and B. Sadaghat, "Automatic calibration of the groundwater simulation model with high parameter dimensionality using sequential uncertainty fitting approach," *Water Supply*, vol. 20, no. 8, pp. 3487–3501, 2020.
[17] J. G. Greener, S. M. Kandathil, L. Moffat, and D. T. Jones, "A guide to machine learning for biologists," *Nat Rev Mol Cell Biol*, vol. 23, no. 1, pp. 40–55, 2022.
[18] H. Chen and L. Zhang, "A machine learning-based method for predicting end-bearing capacity of rock-socketed shafts," *Rock Mech Rock Eng*, vol. 55, no. 3, pp. 1743–1757, 2022.
[19] M. R. Akbarzadeh, H. Ghafourian, A. Anvari, R. Pourhanasa, and M. L. Nehdi, "Estimating Compressive Strength of Concrete Using Neural Electromagnetic Field Optimization," *Materials*, vol. 16, no. 11, p. 4200, 2023.
[20] B. Schölkopf, "Causality for machine learning," in *Probabilistic and Causal Inference: The Works of Judea Pearl*, 2022, pp. 765–804.
[21] S. Z. Sarothi, K. S. Ahmed, N. I. Khan, A. Ahmed, and M. L. Nehdi, "Predicting bearing capacity of double shear bolted connections using machine learning," *Eng Struct*, vol. 251, p. 113497, 2022.
[22] Z.-H. Zhou, *Machine learning*. Springer Nature, 2021.
[23] H. Wang, Z. Lei, X. Zhang, B. Zhou, and J. Peng, "Machine learning basics," *Deep learning*, pp. 98–164, 2016.
[24] M. Meenakshi, "Machine learning algorithms and their real-life applications: A survey," in *Proceedings of the International Conference on Innovative Computing & Communications (ICICC)*, 2020.
[25] T. Onsree and N. Tippayawong, "Machine learning application to predict yields of solid products from biomass torrefaction," *Renew Energy*, vol. 167, pp. 425–432, 2021.
[26] S. C. Jong, D. E. L. Ong, and E. Oh, "State-of-the-art review of geotechnical-driven artificial intelligence techniques in underground soil-structure interaction," *Tunnelling and Underground Space Technology*, vol. 113, p. 103946, 2021.
[27] S. Gao, Y. Hu, X. Zhang, and F. Liu, "Study on tensile mechanical properties of steel strand considering the damage," in *Civil Engineering and Energy-Environment Vol 1: Proceedings of the 4th International Conference on Civil Engineering, Environment Resources and Energy Materials (CCESEM 2022), Sanya, China, 21-23 October 2022*, CRC Press, 2023.
[28] V. Panwar and R. K. Dutta, "Application of Machine Learning Technique in Predicting the Bearing Capacity of Rectangular Footing on Layered Sand under Inclined Loading.," *Journal of Soft Computing in Civil Engineering*, vol. 6, no. 4, 2022.
[29] W. Chen, P. Sarir, X.-N. Bui, H. Nguyen, M. M. Tahir, and D. Jahed Armaghani, "Neuro-genetic,

neuro-imperialism and genetic programing models in predicting ultimate bearing capacity of pile," *Eng Comput*, vol. 36, pp. 1101–1115, 2020.

[30] L. Zhang and J.-J. Chen, "Effect of spatial correlation of standard penetration test (SPT) data on bearing capacity of driven piles in sand," *Canadian Geotechnical Journal*, vol. 49, no. 4, pp. 394–402, 2012.

[31] M. A. Shahin, "Intelligent computing for modeling axial capacity of pile foundations," *Canadian Geotechnical Journal*, vol. 47, no. 2, pp. 230–243, 2010.

[32] C. Sammut and G. I. Webb, *Encyclopedia of machine learning*. Springer Science & Business Media, 2011.

[33] I. Das, A. Stein, N. Kerle, and V. K. Dadhwal, "Landslide susceptibility mapping along road corridors in the Indian Himalayas using Bayesian logistic regression models," *Geomorphology*, vol. 179, pp. 116–125, 2012.

[34] J. Wang, Y. Li, G. Hu, and M. Yang, "An enhanced artificial hummingbird algorithm and its application in truss topology engineering optimization," *Advanced Engineering Informatics*, vol. 54, p. 101761, 2022.

[35] W. Zhao, L. Wang, and S. Mirjalili, "Artificial hummingbird algorithm: A new bio-inspired optimizer with its engineering applications," *Comput Methods Appl Mech Eng*, vol. 388, p. 114194, 2022.

[36] A. Ramadan, S. Kamel, M. H. Hassan, E. M. Ahmed, and H. M. Hasanien, "Accurate photovoltaic models based on an adaptive opposition artificial hummingbird algorithm," *Electronics (Basel)*, vol. 11, no. 3, p. 318, 2022.

[37] M. S. Abid, H. J. Apon, K. A. Morshed, and A. Ahmed, "Optimal planning of multiple renewable energy-integrated distribution system with uncertainties using artificial hummingbird algorithm," *IEEE Access*, vol. 10, pp. 40716–40730, 2022.

[38] W. Zhao, Z. Zhang, S. Mirjalili, L. Wang, N. Khodadadi, and S. M. Mirjalili, "An effective multi-objective artificial hummingbird algorithm with dynamic elimination-based crowding distance for solving engineering design problems," *Comput Methods Appl Mech Eng*, vol. 398, p. 115223, 2022.

[39] A. Fathy, "A novel artificial hummingbird algorithm for integrating renewable based biomass distributed generators in radial distribution systems," *Appl Energy*, vol. 323, p. 119605, 2022.

[40] M. H. Nadimi-Shahraki, S. Taghian, and S. Mirjalili, "An improved grey wolf optimizer for solving engineering problems," *Expert Syst Appl*, vol. 166, p. 113917, 2021.

[41] Z.-M. Gao and J. Zhao, "An improved grey wolf optimization algorithm with variable weights," *Comput Intell Neurosci*, vol. 2019, 2019.